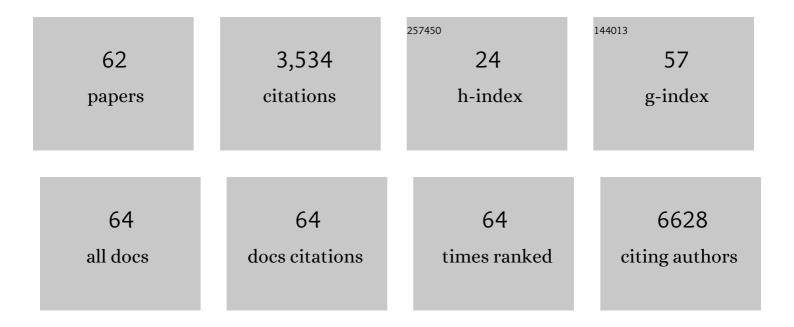
Eric Prestat

List of Publications by Year in descending order

Source: https://exaly.com/author-pdf/7822388/publications.pdf Version: 2024-02-01



FDIC DDESTAT

#	Article	IF	CITATIONS
1	Reply to: Random interstratification in hydrated graphene oxide membranes and implications for seawater desalination. Nature Nanotechnology, 2022, 17, 134-135.	31.5	5
2	Self-Assembled 1T-MoS ₂ /Functionalized Graphene Composite Electrodes for Supercapacitor Devices. ACS Applied Energy Materials, 2022, 5, 61-70.	5.1	31
3	Free, flexible and fast: Orientation mapping using the multi-core and GPU-accelerated template matching capabilities in the Python-based open source 4D-STEM analysis toolbox Pyxem. Ultramicroscopy, 2022, 237, 113517.	1.9	17
4	Enhanced liquid phase exfoliation of graphene in water using an insoluble bis-pyrene stabiliser. Faraday Discussions, 2021, 227, 46-60.	3.2	12
5	lron-silica interaction during reduction of precipitated silica-promoted iron oxides using in situ XRD and TEM. Applied Catalysis A: General, 2021, 613, 118031.	4.3	6
6	Potential dependent ionic sieving through functionalized laminar MoS ₂ membranes. 2D Materials, 2020, 7, 015030.	4.4	21
7	Correlative Microscopy: Elucidating the Mechanisms of SCC in Structural Alloys in PWR Environments. Microscopy and Microanalysis, 2020, 26, 168-170.	0.4	Ο
8	Splenic Capture and <i>In Vivo</i> Intracellular Biodegradation of Biological-Grade Graphene Oxide Sheets. ACS Nano, 2020, 14, 10168-10186.	14.6	51
9	Application of Modern Scanning/Transmission Electron Microscope with Pixelated STEM Detector for Radiation Damage Study. Microscopy and Microanalysis, 2020, 26, 394-395.	0.4	0
10	Stable, concentrated, biocompatible, and defect-free graphene dispersions with positive charge. Nanoscale, 2020, 12, 12383-12394.	5.6	23
11	Convergent beam electron diffraction of multilayer Van der Waals structures. Ultramicroscopy, 2020, 212, 112976.	1.9	6
12	Electrically pumped WSe2-based light-emitting van der Waals heterostructures embedded in monolithic dielectric microcavities. 2D Materials, 2020, 7, 031006.	4.4	16
13	Holographic reconstruction of the interlayer distance of bilayer two-dimensional crystal samples from their convergent beam electron diffraction patterns. Ultramicroscopy, 2020, 219, 113020.	1.9	2
14	Cation-controlled wetting properties of vermiculite membranes and its promise for fouling resistant oil–water separation. Nature Communications, 2020, 11, 1097.	12.8	89
15	Morphological and compositional changes of MFe2O4@Co3O4 (M = Ni, Zn) core-shell nanoparticles after mild reduction. Materials Characterization, 2019, 155, 109806.	4.4	5
16	Enhanced Intraliposomal Metallic Nanoparticle Payload Capacity Using Microfluidic-Assisted Self-Assembly. Langmuir, 2019, 35, 13318-13331.	3.5	14
17	TEM Specimen Preparation Using a Low Energy Ion Beam for Nuclear Metallic Materials. Microscopy and Microanalysis, 2019, 25, 1608-1609.	0.4	1
18	Self-Limiting Growth of Two-Dimensional Palladium between Graphene Oxide Layers. Nano Letters, 2019, 19, 4678-4683.	9.1	18

ERIC PRESTAT

#	Article	IF	CITATIONS
19	Synergistic enhancement of gas selectivity in thin film composite membranes of PIM-1. Journal of Materials Chemistry A, 2019, 7, 6417-6430.	10.3	55
20	Convergent and divergent beam electron holography and reconstruction of adsorbates on free-standing two-dimensional crystals. Frontiers of Physics, 2019, 14, 1.	5.0	7
21	Fate of Lu(III) sorbed on 2-line ferrihydrite at pHÂ5.7 and aged for 12Âyears at room temperature. II: insights from STEM-EDXS and DFT calculations. Environmental Science and Pollution Research, 2019, 26, 5282-5293.	5.3	4
22	Long-range oriented graphene-like nanosheets with corrugated structure. Chemical Communications, 2018, 54, 13543-13546.	4.1	3
23	Study on the formation of thin film nanocomposite (TFN) membranes of polymers of intrinsic microporosity and graphene-like fillers: Effect of lateral flake size and chemical functionalization. Journal of Membrane Science, 2018, 565, 390-401.	8.2	38
24	Corrosion performance of Ti3SiC2, Ti3AlC2, Ti2AlC and Cr2AlC MAX phases in simulated primary water conditions. Corrosion Science, 2018, 139, 444-453.	6.6	41
25	Convergent beam electron holography for analysis of van der Waals heterostructures. Proceedings of the National Academy of Sciences of the United States of America, 2018, 115, 7473-7478.	7.1	17
26	Scalable Patterning of Encapsulated Black Phosphorus. Nano Letters, 2018, 18, 5373-5381.	9.1	43
27	Exploring Environmental Reactions in "Real World" Materials using In Situ Analytical TEM. Microscopy and Microanalysis, 2018, 24, 292-293.	0.4	21
28	Exploring Nanoscale Precursor Reactions in Alloy 600 in H2/N2–H2O Vapor Using In Situ Analytical Transmission Electron Microscopy. Minerals, Metals and Materials Series, 2018, , 399-407.	0.4	0
29	The application of in situ analytical transmission electron microscopy to the study of preferential intergranular oxidation in Alloy 600. Ultramicroscopy, 2017, 176, 46-51.	1.9	37
30	A simple electrochemical route to metallic phase trilayer MoS ₂ : evaluation as electrocatalysts and supercapacitors. Journal of Materials Chemistry A, 2017, 5, 11316-11330.	10.3	119
31	Tunable sieving of ions using graphene oxide membranes. Nature Nanotechnology, 2017, 12, 546-550.	31.5	1,364
32	Enhanced organophilic separations with mixed matrix membranes of polymers of intrinsic microporosity and graphene-like fillers. Journal of Membrane Science, 2017, 526, 437-449.	8.2	57
33	Role of 2D and 3D defects on the reduction of LaNiO3 nanoparticles for catalysis. Scientific Reports, 2017, 7, 10080.	3.3	27
34	Desalination and Nanofiltration through Functionalized Laminar MoS ₂ Membranes. ACS Nano, 2017, 11, 11082-11090.	14.6	275
35	Understanding 2D Crystal Vertical Heterostructures at the Atomic Scale Using Advanced Scanning Transmission Electron Microscopy. Microscopy and Microanalysis, 2017, 23, 1714-1715.	0.4	0
36	An in situ and ex situ TEM study into the oxidation of titanium (IV) sulphide. Npj 2D Materials and Applications, 2017, 1, .	7.9	21

Eric Prestat

#	Article	IF	CITATIONS
37	Plasmon-induced nanoscale quantised conductance filaments. Scientific Reports, 2017, 7, 2878.	3.3	3
38	Mapping grain boundary heterogeneity at the nanoscale in a positive temperature coefficient of resistivity ceramic. APL Materials, 2017, 5, 066105.	5.1	11
39	Electron Microscopy (Big and Small) Data Analysis With the Open Source Software Package HyperSpy. Microscopy and Microanalysis, 2017, 23, 214-215.	0.4	74
40	Observing Imperfection in Atomic Interfaces for van der Waals Heterostructures. Nano Letters, 2017, 17, 5222-5228.	9.1	53
41	Real Time Evolution of the Reduction of Ilmenite in H2: A Correlative In Situ and Ex Situ Study. Microscopy and Microanalysis, 2016, 22, 54-55.	0.4	0
42	Imaging the Hydrated Microbe-Metal Interface Using Nanoscale Spectrum Imaging. Particle and Particle Systems Characterization, 2016, 33, 833-841.	2.3	2
43	Temperature Programmed Reduction of a PdCu Bimetallic Catalyst via Atmospheric Pressure in situ STEM-EDS and in situ X-Ray Adsorption Analysis. Microscopy and Microanalysis, 2016, 22, 214-215.	0.4	1
44	The Effects of Extensive Glomerular Filtration of Thin Graphene Oxide Sheets on Kidney Physiology. ACS Nano, 2016, 10, 10753-10767.	14.6	70
45	Self-catalytic membrane photo-reactor made of carbon nitride nanosheets. Journal of Materials Chemistry A, 2016, 4, 11666-11671.	10.3	47
46	Van der Waals pressure and its effect on trapped interlayer molecules. Nature Communications, 2016, 7, 12168.	12.8	137
47	Synthesis and characterization of composite membranes made of graphene and polymers of intrinsic microporosity. Carbon, 2016, 102, 357-366.	10.3	34
48	Cross sectional STEM imaging and analysis of multilayered two dimensional crystal heterostructure devices. Microscopy and Microanalysis, 2015, 21, 107-108.	0.4	1
49	Core-shell nanostructure in a <mml:math xmlns:mml="http://www.w3.org/1998/Math/MathML"><mml:mrow><mml:msub><mml:mi>Ge</mml:mi><mml:r observed via structural and magnetic measurements. Physical Review B, 2015, 91, .</mml:r </mml:msub></mml:mrow></mml:math 	nr ଊ୶ ୰ <mi< td=""><td>ทl:ลาท>0.9</td></mi<>	ทl: ล าท>0.9
50	In situ Analytical TEM of Ilmenite Reduction in Hydrogen. Microscopy and Microanalysis, 2015, 21, 565-566.	0.4	2
51	XEDS and EELS in the TEM at Atmospheric Pressure and High Temperature. Microscopy and Microanalysis, 2015, 21, 247-248.	0.4	8
52	Quality Heterostructures from Two-Dimensional Crystals Unstable in Air by Their Assembly in Inert Atmosphere. Nano Letters, 2015, 15, 4914-4921.	9.1	358
53	Investigations of segregation phenomena in highly strained Mn-doped Ge wetting layers and Ge quantum dots embedded in silicon. Applied Physics Letters, 2014, 104, 102409.	3.3	1
54	Real-time imaging and elemental mapping of AgAu nanoparticle transformations. Nanoscale, 2014, 6, 13598-13605.	5.6	64

ERIC PRESTAT

#	Article	IF	CITATIONS
55	Coarsening of Pt nanoparticles on amorphous carbon film. Surface Science, 2013, 609, 195-202.	1.9	11
56	Structure and magnetism in strained Ge1â^'‹i>x‹/i>â^'‹i>y‹/i>Sn‹i>x‹/i>Mn‹i>y‹/i> films grown on Ge(001) by low temperature molecular beam epitaxy. Applied Physics Letters, 2013, 103, .	3.3	1
57	Advanced semiconductor characterization with aberration corrected electron microscopes. Journal of Physics: Conference Series, 2013, 471, 012001.	0.4	3
58	Electrical and thermal spin accumulation in germanium. Applied Physics Letters, 2012, 101, .	3.3	28
59	Size Dependence of Exchange Bias in <mml:math <br="" xmlns:mml="http://www.w3.org/1998/Math/MathML">display="inline"><mml:mi>Co</mml:mi><mml:mo>/</mml:mo><mml:mi>CoO</mml:mi></mml:math> Nanostruct Physical Review Letters, 2012, 108, 077205.	u 763.	60
60	Crossover from Spin Accumulation into Interface States to Spin Injection in the Germanium Conduction Band. Physical Review Letters, 2012, 109, 106603.	7.8	76
61	Interface-driven phase separation in multifunctional materials: The case of the ferromagnetic semiconductor GeMn. Physical Review B, 2012, 85, .	3.2	22
62	Composition and morphology of self-organized Mn-rich nanocolumns embedded in Ge: Correlation with the magnetic properties. Journal of Applied Physics, 2012, 112, .	2.5	13